Preprints of the 18th IFAC World Congress
Milano (Italy) August 28 - September 2, 2011

Robust Feedforward control for a Drop-on-Demand Inkjet Printhead ⋆

Amol A. Khalate * **Xavier Bombois** * **Gérard Scorletti** **
Robert Babuška * **René Waarsing** *** **Wim de Zeeuw** ***

* *Delft Center for Systems and Control, Delft University of Technology, Mekelweg 2, 2628 CD Delft, The Netherlands. (email: {a.a.khalate, x.j.a.bombois, r.babuska}@tudelft.nl)*
** *Laboratoire Ampére, Ecole Centrale de Lyon, 36 avenue Guy de Collongue - 69134 Ecully Cedex, France*
*** *Océ Technologies B.V., 5900 MA Venlo, The Netherlands.*

Abstract: The printing quality delivered by a Drop-on-Demand (DoD) inkjet printhead is mainly limited due to the residual oscillations in the ink channel. The maximal jetting frequency of a DoD inkjet printhead can be increased by quickly damping the residual oscillations and by bringing in this way the ink-channel to rest after jetting the ink drop. The inkjet channel model obtained is generally subjected to parametric uncertainty. This paper proposes a robust optimization-based method to design the input actuation waveform for the piezo actuator in order to improve the damping of the residual oscillations in the presence of parametric uncertainties in the ink-channel model. Experimental results are presented to show the efficacy of the proposed method.

1. INTRODUCTION

The ability of inkjet technology to deposit materials with diverse chemical and physical properties has made it an important technology for both industry and home use. Apart from conventional document printing, the inkjet technology has been successfully applied in the areas of electronics, mechanical engineering and life sciences [Williams, 2006]. This is mainly thanks to the low operational costs of the technology. Typically, a drop-on-demand (DoD) inkjet printhead consists of several ink channels in parallel. Each channel is provided with a piezo-actuator, which on application of a voltage pulse can generate pressure oscillations inside the ink channel. These pressure oscillations push the ink drop out of the nozzle. A detailed description of the droplet jetting process can be found in [Wassink, 2007]. The print quality delivered by an inkjet printhead depends on the properties of the jetted drop, i.e., the drop velocity, the jetting direction and the drop volume. To meet the challenging performance requirements posed by new applications, these drop properties have to be tightly controlled.

The performance of the inkjet printhead is mainly limited due to the *residual pressure oscillations*. The actuation pulses are designed to provide an ink drop of a specified volume and velocity under the assumption that the ink channel is in steady state. Once the ink drop is jetted, the pressure oscillations inside the ink channel take several micro-seconds to decay. If the next ink drop is jetted before the residual pressure oscillations settle, the resulting drop properties will be different from the ones of the previous drop. Therefore, at a high jetting frequency, drops will be jetted before the oscillations in the ink channel have completely disappeared and these residual oscillations will influence the drop velocity. This can degrade the printhead performance, since a printhead has to jet drops with a constant velocity at different frequencies. Given this fact, an important characteristic is the so-called DoD curve which represents the ink drop velocity as a function of the jetting frequency (which is also called the DoD frequency). Ideally, the DoD curve must be flat. However, for the above reasons, this DoD curve is far from flat in practice. Our goal in this paper is to flatten the DoD curve by redesigning the piezo actuation pulse.

In the literature, we can find various methods [Bogy and Talke, 1984, Chung et al., 2005, Kwon and Kim, 2007, Kwon, 2009] to design the piezo actuation pulse. In our earlier work [Khalate et al., 2010] we have proposed an optimization-based method to design the actuation pulse. This is a model-based approach and we have used a discrete-time model $H(q)$ relating the piezo input voltage (i.e., the input u) to the velocity of the meniscus (i.e., the output y). The meniscus is an interface between the ink and air. In order to design the piezo actuation pulse with shape constraint, we assume that the possible inputs can be parameterized as $u(k,\theta)$ with θ a parameter vector and k the discrete time index. Based on the reference meniscus velocity template $y_{\text{ref}}(k)$ (i.e., a meniscus velocity profile with fast decaying residual oscillations) and the transfer function $H(q)$, an optimal actuation pulse $u(k,\theta_{\text{opt}})$ is determined as the one minimizing the performance index given as follows

$$\mathcal{J}_{\text{nominal}}(\theta) = \sum_{k=0}^{N} \Big(y_{\text{ref}}(k) - H(q)u(k,\theta) \Big)^2 \qquad (1)$$

⋆ This work has been carried out as part of the Octopus project with Océ Technologies B.V. under the responsibility of the Embedded Systems Institute. This project is partially supported by the Netherlands Ministry of Economic Affairs under the Bsik program

where $N = \frac{T}{T_s}$, T_s is sampling time, T is chosen equal to 100μs, and q is the forward shift operator.

The optimal actuation pulse designed with this method was evaluated on an experimental setup at Océ Technologies, Netherlands. In each experiment we jetted 10 ink drops from the inkjet channel at a fixed DoD frequency. The performance of the optimal actuation pulse $u(k, \theta_{\text{opt}})$ was analyzed using the DoD-curve. This optimization-based method is a feedforward control strategy and hence, it is highly sensitive to model mismatch. The model mismatch is the major reason for the DoD-curve not being completely flat.

The dynamical model $H(q)$ from the piezo input to the meniscus velocity obtained at different DoD frequencies will not be the same. With the help of this set of dynamical models at different DoD frequencies, one can think of designing several optimal actuation pulses, one for every possible operating DoD frequency. In practice, this solution to make the DoD curve flat cannot be implemented due to the hardware limitations. These limitations demand a single actuation pulse to be designed such that its performance is fairly good over the operating range of the DoD frequencies. In this paper, we present a very compact parametric polytopic uncertainty model $\Delta \in \mathbf{\Delta}$, such that the uncertain model $H(q, \Delta)$, encompasses the set of dynamics at various operating DoD frequencies. Thus, the robust actuation pulse can be obtained by minimizing the worst-case norm of the tracking error with the uncertain system $H(q, \Delta)$. The choice of the polytopic uncertainty model enables us to use the classical results on robust H_2 filtering.

2. SYSTEM DESCRIPTION AND MODELING

Several analytic and numerical models are available for the inkjet channel dynamics. For control applications, one prefers a simple model with sufficient accuracy. Therefore, we select a simplified discrete-time model $H(q)$ based on the 'narrow-gap model' [Wijshoff, 2008]. We know that the higher order modes in the meniscus velocity do not contribute significantly to the drop formation process [Dijksman, 1984]. Hence, these higher order modes are neglected in $H(q)$. The discrete-time model $H(q)$ describes the dynamics from the piezo input voltage u to the meniscus velocity y. The transfer function $H(q)$ is given as follows

$$H(q) = g\left(\frac{q^2 + b_1 q + b_2}{q^2 + a_1 q + a_2}\right)\left(\frac{q^2 + b_3 q + b_4}{q^2 + a_3 q + a_4}\right) \qquad (2)$$

where q is the forward shift operator and the nominal values of the coefficients are

$$b_1 = -1.2194, b_2 = 0.2194, b_3 = -1.7170, b_4 = 7.0670,$$
$$a_1 = -1.6480, a_2 = 0.8839, a_3 = -1.0040, a_4 = 0.8971,$$
$$g = -0.0074.$$

The sampling time T_s is chosen equal to 1μs.

Fig. 1 shows the frequency response of the above 4-th order transfer function $H(q)$. This inkjet system can be represented in the state-space form as follows

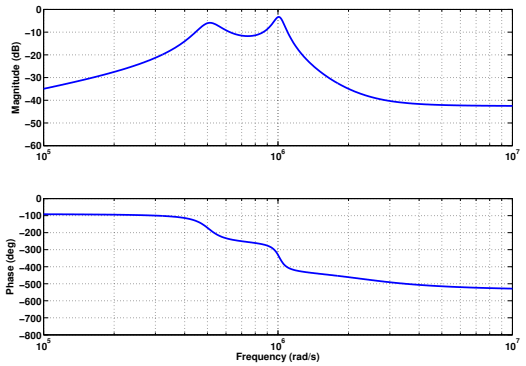

Fig. 1. Frequency response of the transfer function model $H(q)$.

$$x_S(k+1) = A_S x_S(k) + B_S u(k)$$
$$y(k) = C_S x_S(k) + D_S u(k) \qquad (3)$$

where

$$A_S = \begin{bmatrix} -a_1 & -a_2 & 0 & 0 \\ 1 & 0 & 0 & 0 \\ g(b_1 - a_1) & -g(b_2 - a_2) & -a_3 & -a_4 \\ 0 & 0 & 1 & 0 \end{bmatrix}, \quad B_S = \begin{bmatrix} 1 \\ 0 \\ g \\ 0 \end{bmatrix}$$
$$C_S = [g(b_1 - a_1) \ -g(b_2 - a_2) \ (b_3 - a_3) \ (b_4 - a_4)]$$
$$D_S = [g] \, .$$

As discussed in the introduction, at different DoD frequencies, the dynamics from the piezo input to the meniscus velocity $H(q)$ will be not be the same. This may be due to the unmodeled refill dynamics or the nonlinear effects in the drop formation process. In order to investigate this phenomenon, we have used experimental identification. It is very difficult to experimentally measure the meniscus position and the meniscus velocity while jetting an ink drop. However, the piezoelectric crystal can be simultaneously used as an actuator and as a sensor. Therefore, we have identified a dynamical system from the piezo input to the piezo-sensor output (which is proportional to the derivative of the ink-channel pressure) at a fixed DoD frequency. We have done several such experiments at various fixed DoD frequencies in the operating range of the inkjet printhead. The details of the identification experiments are omitted in this paper due to lack of space.

It is observed that the first resonant mode of the inkjet system varies a lot compared to the second resonant mode. Using this information, it can be found that for the first resonant mode of $H(q)$, the resonance frequency variation is approximately in the interval $[-7\% \ + 7\%]$ and the damping variation is approximately in the interval $[-70\% \ +30\%]$. The variation in the second resonant mode is relatively smaller compared to the first one.

One can obtain more realistic uncertainty model around the nominal plant $H(q)$ by considering uncertainty on all the coefficients of the transfer function (2). This helps to reduce the conservatism in the feedforward control design. However, for our problem this will increase the computational burden to compute a robust feedforward controller. Hence, in order to obtain a simpler and more compact uncertainty description we assume that only the first resonant mode is uncertain. This is a valid assumption since the first mode greatly influences the ink

drop properties [Dijksman, 1984] compared to the second mode. The details on the mapping of the uncertainty on the properties of the resonant mode to the coefficients of the transfer function (2) can be found in Appendix A. Due to the uncertain first resonant mode, the coefficients of the T.F. (2), a_1 and a_2 are subjected to uncertainty Δ. The uncertainty $\Delta = [\Delta^{(1)} \ \ \Delta^{(2)}]^T$ perturbs the coefficients a_1 and a_2 in the following manner:

$$a_1(\Delta) = a_{1,\text{nom}}(1 + \Delta^{(1)}) \tag{4}$$

$$a_2(\Delta) = a_{2,\text{nom}}(1 + \Delta^{(2)}), \tag{5}$$

where $a_{1,\text{nom}} = -1.6480$ and $a_{2,\text{nom}} = 0.8839$ are the nominal values of the coefficients a_1 and a_2. The uncertainty Δ on the coefficients lie inside the polytope $\mathbf{\Delta}$ which is formed by convex combination of the four vertices $\Delta_i,\ i = 1, 2, 3, 4$, i.e. $\Delta \in \mathbf{\Delta}$= conv$(\Delta_1, \Delta_2, \Delta_3, \Delta_4)$. The values of $\Delta_1, ..., \Delta_4$ can be found in the Appendix A. This choice of uncertainty enables us to use classical results available in the literature.

It can be seen that the uncertainty Δ enters linearly in the matrices (3). Thus, the matrices of the inkjet system $H(q, \Delta)$ for the admissible uncertainty $\Delta \in \mathbf{\Delta}$ belong to the polytope

$$\Big(A_s(\Delta), B_s(\Delta), C_s(\Delta), D_s(\Delta)\Big) = \sum_{i=1}^{4} \alpha_i \big(A_{s_i}, B_{s_i}, C_{s_i}, D_{s_i}\big), \tag{6}$$

where the matrices $A_{s_i} = A_s(\Delta_i)$, $B_{s_i} = B_s(\Delta_i)$, $C_{s_i} = C_s(\Delta_i)$, $D_{s_i} = D_s(\Delta_i), i = 1, 2, 3, 4$, are the system matrices of a fixed inkjet system at the i-th vertex of the polytope and α_i are positive scalars such that $\sum_{i=1}^{4} \alpha_i = 1$. In the next section, we use this uncertain model of the inkjet system $H(q, \Delta)$ in order to design a robust actuation pulse.

3. FEEDFORWARD CONTROL DESIGN

In our previous work, [Khalate et al., 2010], we have designed a template for the desired meniscus velocity $y_{\text{ref}}(k)$, i.e., a meniscus velocity profile with fast decaying residual oscillations. If the actuation pulse $u(k)$ is designed in such a way that the meniscus velocity $y(k)$ follows the reference trajectory $y_{\text{ref}}(k)$, then the channel will come to rest very quickly after jetting the ink drop. This will create the condition to jet the ink drops at higher jetting frequencies. As discussed in the introduction, the optimization-based method [Khalate et al., 2010] poses difficulties in the presence of model mismatch. Therefore, to improve the robustness of the feedforward controller we propose to recast the problem as a model matching or filtering problem (see Fig.2).

In the previous Section, the model mismatch has been described as a compact polytopic uncertainty. This uncertainty in the inkjet channel model can now be handled owing to the H_2 filtering formulation discussed below. A robust actuation pulse is obtained as the one minimizing the square of the worst-case H_2 norm of the tracking error transfer function. In this section, we first present the design of an unconstrained robust actuation pulse and subsequently, its extension to the design of a constrained robust actuation pulse.

3.1 Unconstrained Robust Feedforward Control

For many inkjet printheads, the actuation pulse with shape constraints may not be very close to the optimal unconstrained pulse. The performance degradation resulting by imposing the shape constraints on the actuation pulse may become significant. This may enforce the inkjet printhead manufacturer to relax the shape constraints on the actuation pulse. Rapid developments in the electronics field enables them to use more sophisticated electronic hardware which can generate an unconstrained actuation pulse. Therefore, it is essential to investigate the possibility of an unconstrained actuation pulse which will damp the residual oscillations when the inkjet channel model is subjected to parametric uncertainty. Hence, we first formulate the feedforward control problem as a filtering problem. As shown in Fig. 2, we use the model $H_{\text{ref}}(q)$ to generate the the reference trajectory $y_{\text{ref}}(k)$. Design of the model $H_{\text{ref}}(q)$ is simpler once we chose a finite impulse response (FIR) model structure for it.

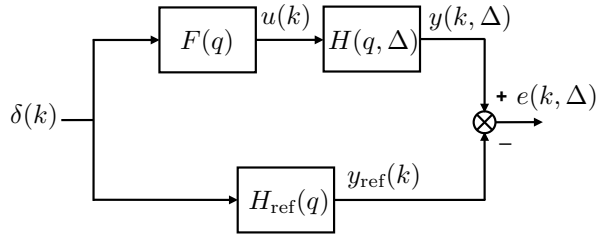

Fig. 2. Filtering problem for the inkjet printhead.

The state-space representation of the reference model $H_{\text{ref}}(q)$ is given as follows

$$\begin{aligned} x_R(k+1) &= A_R x_R(k) + B_R \delta(k) \\ y_{ref}(k) &= C_R x_R(k) + D_R \delta(k) \end{aligned} \tag{7}$$

where $\delta(k)$ is the unit pulse.

We also parameterize the actuation pulse as the pulse response of a FIR filter $F(q, \beta)$:

$$u(k) = F(q, \beta)\delta(k) \tag{8}$$

with $F(q, \beta) = \beta_0 + \beta_1 q^{-1} + \cdots + \beta_{n_f} q^{-n_f}$, $\beta = [\beta_0, \ldots, \beta_{n_f}]^T$ a vector containing the coefficients of the FIR filter and $\delta(k)$ the unit pulse. The state-space representation of $F(q, \beta)$ is given as follows

$$\begin{aligned} x_F(k+1) &= A_F x_F(k) + B_F \delta(k) \\ u(k, \beta) &= C_F(\beta) x_F(k) + D_F(\beta)\delta(k) \end{aligned} \tag{9}$$

where

$$A_F = \begin{bmatrix} 0 & 0 \\ I_{n_f-1} & 0 \end{bmatrix}, \quad B_F = \begin{bmatrix} 1 \\ 0 \end{bmatrix}$$

$$C_F(\beta) = \begin{bmatrix} \beta_1 & \cdots & \beta_{n_f} \end{bmatrix}, \quad D_F(\beta) = \beta_0.$$

The choice of the filter structure is important, as it determines the length and the shape of the actuation pulse. One can choose the filter $F(q)$ as a rational function, however, this would result in an actuation pulse of an infinite length because the rational filter has an infinite pulse response. However, in our problem, it is required to obtain a finite length actuation pulse. The use of the FIR structure allows us to set the length of the actuation pulse a-priori. In addition, the to-be-designed filter coefficient vector β only appears in the state-space matrices C_F

and D_F. This property greatly simplifies the optimization problem to design the filter $F(q)$.

Note that the inkjet system $H(q,\Delta)$ is a single input single output (SISO) system. Hence, the uncertain error dynamics $\nu(q,\beta,\Delta) = \big(H_{\text{ref}}(q) - H(q,\Delta)F(q,\beta)\big)$ will not be changed if we interchange $H(q,\Delta)$ and $F(q)$, i.e. $\nu(q,\beta,\Delta) = \big(H_{\text{ref}}(q) - F(q,\beta)H(q,\Delta)\big)$, see Fig. 2. Thus, the state-space representation of the error dynamics $\nu(q,\beta,\Delta)$ is given as follows

$$\begin{aligned} x(k+1) &= A(\Delta)x(k) + B(\Delta)\delta(k) \\ e(k,\beta,\Delta) &= C(\beta,\Delta)x(k) + D(\beta,\Delta)\delta(k), \end{aligned} \tag{10}$$

where

$$A(\Delta) = \begin{bmatrix} A_S(\Delta) & 0 & 0 \\ B_F C_S(\Delta) & A_F & 0 \\ 0 & 0 & A_R \end{bmatrix}, B(\Delta) = \begin{bmatrix} B_S(\Delta) \\ B_F D_S(\Delta) \\ B_R \end{bmatrix}$$
$$C(\beta,\Delta) = [\, -D_F(\beta)C_S(\Delta) \;\; -C_F(\beta) \;\; C_R \,],$$
$$D(\beta,\Delta) = [\, D_R - D_F(\beta)D_S(\Delta) \,].$$

It can be seen that thanks to the particular choice of the FIR structure for the filter $F(q)$, only the matrices C and D of (10) depend on the filter coefficient vector β. Also, as we assume the uncertainty Δ to be of a polytopic nature ($\Delta \in \boldsymbol{\Delta}$), the state-space matrices of the error system $\nu(q,\beta,\Delta)$ belong to following polytope

$$\begin{aligned} &\Big(A(\Delta), B(\Delta), C(\beta,\Delta), D(\beta,\Delta)\Big) \\ &= \sum_{i=1}^{4} \alpha_i \big(A_i, B_i, C_i(\beta), D_i(\beta)\big). \end{aligned} \tag{11}$$

where the matrices $\big(A_i, B_i, C_i(\beta), D_i(\beta)\big)$ are the state-space matrices of the fixed error dynamics $\nu_i(q,\beta)$ at the i-th vertex of the polytope and α_i are positive scalars such that $\sum_{i=1}^{4} \alpha_i = 1$. Clearly, the uncertain system error dynamics is a convex combination of the fixed systems at the vertices of the polytope $\boldsymbol{\Delta}$.

As discussed in the introduction, in our earlier work [Khalate et al., 2010], the performance index (1) for the actuation pulse is defined as the square of the H_2 norm of the tracking error. Now, the inkjet system is perturbed by the uncertainty $\Delta \in \boldsymbol{\Delta}$. Therefore, we define the performance index $\mathcal{J}(\beta)$ as the square of the worst-case H_2 norm of the tracking error transfer function $\nu(q,\beta,\Delta)$:

$$\begin{aligned} \mathcal{J}(\beta) &= \max_{\Delta\in\boldsymbol{\Delta}} \big\|\nu(q,\beta,\Delta)\big\|_2^2 \\ &= \max_{\Delta\in\boldsymbol{\Delta}} \big\|H_{\text{ref}}(q) - H(q,\Delta)F(q,\beta)\big\|_2^2. \end{aligned} \tag{12}$$

The filter coefficient vector β_{robust}, describing the unconstrained robust actuation pulse is thus the solution β_{robust} of the following optimization problem

$$\begin{aligned} \beta_{\text{robust}} &= \arg\min_{\gamma,\ \beta} \gamma \\ \text{subject to} \quad & \mathcal{J}(\beta) < \gamma. \end{aligned} \tag{13}$$

The robust actuation pulse defined as the solution of the above optimization can be obtained using the following Proposition.

Note that we use $*$ as an ellipsis for terms that can be induced by symmetry.

Proposition 1. Consider the error dynamics given by (10) then, the optimal coefficient vector β_{robust} for the robust actuation pulse can be determined by solving the following LMI optimization

$$\beta_{\text{robust}} = \min_{\gamma^{\text{UB}},\ \beta,\ K=K^T} \gamma^{\text{UB}}$$

$$\text{subject to} \quad \begin{bmatrix} \gamma^{\text{UB}} - B_i^T K B_i & * \\ D_i(\beta) & 1 \end{bmatrix} > 0 \tag{14}$$

$$\begin{bmatrix} K - A_i^T K A_i & * \\ C_i(\beta) & 1 \end{bmatrix} > 0, \quad i = 1,2,3,4, \tag{15}$$

with A_i, B_i, C_i, D_i defined in (11).

Indeed, the above optimization problem delivers an upper bound $\gamma^{\text{UB}}_{\text{opt}}$ for the optimal γ of the problem (13).

Proof: Consider the system (10) for one particular Δ and for one particular β. Then, following the same reasoning as e.g. in the proof of Proposition 2 in [Bombois et al., 2010], it can be shown that $\|\nu(q,\beta,\Delta)\|_2^2 < \gamma^{\text{UB}}$ if there exists a positive definite symmetric matrix K such that

$$\begin{aligned} B(\Delta)^T K B(\Delta) + D^2(\beta,\Delta) &< \gamma^{\text{UB}} \\ A(\Delta)^T K A(\Delta) + C^T(\beta,\Delta)C(\beta,\Delta) &< K \end{aligned} \tag{16}$$

These two LMIs can also be rewritten as follows using Schur's complement

$$\begin{bmatrix} \gamma^{\text{UB}} & * & * \\ B(\Delta) & K^{-1} & * \\ D(\beta,\Delta) & 0 & 1 \end{bmatrix} > 0, \begin{bmatrix} K & * & * \\ A(\Delta) & K^{-1} & * \\ C(\beta,\Delta) & 0 & 1 \end{bmatrix} > 0. \tag{17}$$

The LMIs (17) are affine in Δ because the matrices $A(\Delta), B(\Delta), C(\beta,\Delta), D(\beta,\Delta)$ are affine in Δ. In [Boyd et al., 1994], it is shown that (17) hold for all $\Delta \in \boldsymbol{\Delta}$ if (17) hold for $\Delta = \Delta_i,\ i = 1,...,4$; in other words if the following LMIs hold

$$\begin{bmatrix} \gamma^{\text{UB}} & * & * \\ B_i & K^{-1} & * \\ D_i(\beta) & 0 & 1 \end{bmatrix} > 0, \begin{bmatrix} K & * & * \\ A_i & K^{-1} & * \\ C_i(\beta) & 0 & 1 \end{bmatrix} > 0\ , \tag{18}$$

for $i = 1,2,3,4$. Using the Schur's complement, (18) reduces to (14) and (15).

Note finally that the expressions (14) and (15) are LMIs in β since C and D in (10) are affine in C_F and D_F in (9). The matrices C_F and D_F are indeed also linear function of β. ■

3.2 Constrained Robust Feedforward Control

In order to use the unconstrained robust actuation pulse, the printhead would need a new sophisticated electronic hardware. Since, most of the printheads can only generate a constrained actuation pulse (i.e., the shape of the actuation pulse restricted to trapezoid), we investigate the possibility of obtaining a constrained feedforward control by restricting the coefficients of the FIR filter. Similar to [Khalate et al., 2010], we parameterize the constrained actuation pulse $u(k,\theta)$ using the parameter vector $\theta = [t_{r_R}\ t_{w_R}\ t_{f_R}\ V_R\ t_{d_Q}\ t_{r_Q}\ t_{w_Q}\ t_{f_Q}\ V_Q]^T$ as shown in Fig. 3. In order to design the robust trapezoidal actuation pulse, we restrict the coefficients of the FIR filter $F(q,\beta(\theta))$ such that

$$u(k,\theta) = F(q,\beta(\theta))\delta(k) \tag{19}$$

where $\beta(\theta)$ is the filter coefficient vector, which nonlinearly depends on the trapezoidal pulse parameter vector θ and $\delta(k)$ is the unit pulse.

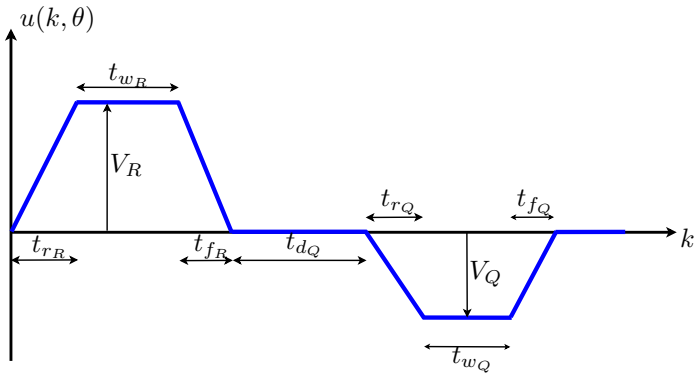

Fig. 3. Proposed piezo actuation pulse.

Now, the performance index $\mathcal{J}(\theta)$, which is defined as the square of the worst-case H_2 norm of the tracking error transfer function $\nu(q,\beta(\theta),\Delta)$ is given as follows

$$\mathcal{J}(\theta) = \max_{\Delta\in\mathbf{\Delta}} \left\| H_{\text{ref}}(q) - H(q,\Delta)F(q,\beta(\theta)) \right\|_2^2. \qquad (20)$$

For a given parameter vector θ, we can obtain an upper bound $\mathcal{J}_{\text{UB}}(\theta)$ on the performance index $\mathcal{J}(\theta)$ using the optimization problem in Proposition 1. Here, we solve the optimization problem (14)-(15) with a fixed β associated with θ to obtain the optimal γ^{UB}. Indeed, we have $\mathcal{J}_{\text{UB}}(\theta) = \gamma^{\text{UB}}_{\text{opt}}$, with $\gamma^{\text{UB}}_{\text{opt}}$ the optimal γ^{UB} corresponding to the optimization problem in Proposition 1.

However, as the dimension of the parameter space of Δ is small, we can also easily grid the parametric uncertainty $\mathbf{\Delta}$. Let the set $\mathcal{S}$ be the grid on the parametric uncertainty $\mathbf{\Delta}$, defined as

$$\mathcal{S} = \{\Delta^i, i = 1, ..., m, \mid \Delta^i \in \mathbf{\Delta}\}$$

Thus, a lower bound $\mathcal{J}_{\text{LB}}(\theta)$ on the performance index $\mathcal{J}(\theta)$ can be obtained easily by computing the H_2 norm at each of the m grid elements, i.e.:

$$\mathcal{J}_{\text{LB}}(\theta) = \max_{\Delta^i\in\mathcal{S}} \left\| H_{\text{ref}}(q) - H(q,\Delta^i)F(q,\beta(\theta)) \right\|_2^2. \qquad (21)$$

In order to obtain the robust actuation pulse one can minimize either $\mathcal{J}_{\text{UB}}(\theta)$ or $\mathcal{J}_{\text{LB}}(\theta)$. In the sequel, we will choose $\mathcal{J}_{\text{LB}}(\theta)$.

Now, the constrained robust actuation pulse parameter is thus the solution θ_{robust} of the following optimization problem

$$\min_{\gamma,\theta} \gamma$$
$$\text{subject to} \quad \mathcal{J}_{\text{LB}}(\theta) < \gamma \quad \text{and} \quad \theta_{LB} \le \theta \le \theta_{UB}, \qquad (22)$$

where, θ_{LB} and θ_{UB} are the vectors containing the lower and the upper bounds on each element of the parameter vector θ.

This is a nonlinear optimization problem and can be solved offline using standard optimization algorithms. We use gradient-based optimization for this purpose. Gradient-based optimization is an iterative method. The gradient of $\mathcal{J}_{\text{LB}}(\theta)$ is computed numerically around the current value of θ and then the parameter θ is updated in the gradient direction.

4. EXPERIMENTAL RESULTS

In this section, we present experimental results to show the improvements in the drop consistency with the robust actuation pulse. We have solved the robust unconstrained actuation problem (14)-(15) using the LMI toolbox of MATLAB. However, as only a constrained actuation pulse can be used in the current printhead, we have not used the unconstrained actuation pulse for the experiment. In order to obtain the constrained robust actuation pulse, the nonlinear optimization problem (22) is solved by using the command `fmincon` from the optimization toolbox of MATLAB. We used a fine grid $\mathcal{S}$ on the uncertainty parameter space $\mathbf{\Delta}$ to compute the lower bound on the performance index $\mathcal{J}_{\text{LB}}(\theta)$. The robust actuation pulse parameter vector θ_{robust} obtained after solving the optimization problem (22) is

$$\theta_{\text{robust}} = [1.5\ 2.5\ 1.5\ 23.0\ 6.93\ 2.74\ 0.4\ 3.75\ -13.22]^T$$

Note that in the parameter vector θ, the time parameters (t_r, t_w, t_f, t_{d_Q}) of the actuation pulse are expressed in μs. The parameter vector θ_{robust} is provided to the computational unit of the printhead to generate the robust pulse $u_{\text{robust}}(k) = u(k,\theta_{\text{robust}})$.

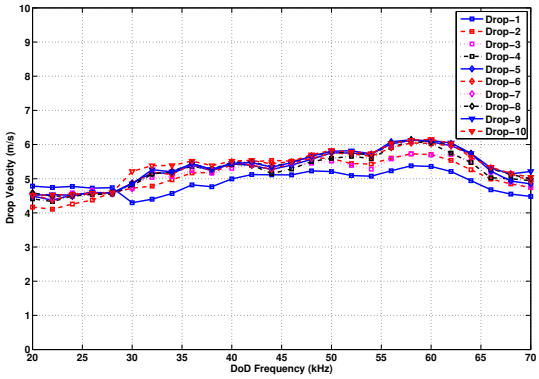

Fig. 4. Experimental DoD curve with the constrained robust pulse.

In each experiment we have jetted 10 ink drops from the inkjet channel at a fixed DoD frequency using the robust pulse $u_{\text{robust}}(k)$. The drop velocities of each of the ten drops are shown in Fig.4 as a function of the DoD frequency (DoD curve) when the robust actuation pulse is used. It is evident that the DoD-curve with the robust pulse is considerably flatter compared to the DoD curve with the optimal pulse [Khalate et al., 2010]. The overall improvement in the velocity consistency achieved using the robust actuation pulse has a far reaching consequence for the print quality. This is because of the proximity of the inkjet printhead to the printing paper.

5. CONCLUSION

In this paper, we have proposed a compact description of the model mismatch in the inkjet-channel model as a parametric uncertainty. In order to damp the residual oscillations in the presence of this parametric uncertainty, two optimization-based approches to design a constrained and an unconstrained robust actuation pulse are developed using the robust H_2 filtering framework. Experimental results have demonstrated that a considerable improvement in the ink drop consistency can be achieved with the proposed constrained robust pulse. Applications of the

proposed method to multi-channel control will be investigated in the future.

ACKNOWLEDGEMENTS

The authors gratefully acknowledge fruitful discussions with S. H. Koekebakker, P. Klerken, Herman Wijshoff and experimental support from J. Simons .

REFERENCES

D.B. Bogy and F.E. Talke. Experimental and theoretical study of wave propagation phenomena in drop-on-demand ink jet devices. *IBM J. Res. Dev.*, 28(3):314–321, 1984.

X.J.A. Bombois, H. Hjalmarsson, and G. Scorletti. Identification for robust H_2 deconvolution filtering. *Automatica*, 46(3):577 – 584, 2010.

S. Boyd, L. El Ghaoui, E. Feron, and V. Balakrishnan. *Linear Matrix Inequalities in System and Control Theory*, volume 15 of *Studies in Applied Mathematics*. SIAM, Philadelphia, PA, June 1994. ISBN 0-89871-334-X.

J. Chung, S. Ko, C.P. Grigoropoulos, N.R. Bieri, C. Dockendorf, and D. Poulikakos. Damage-Free low temperature pulsed laser printing of gold nanoinks on polymers. *Journal of Heat Transfer*, 127(7):724–732, July 2005.

J.F. Dijksman. Hydrodynamics of small tubular pumps. *Journal of Fluid Mechanics*, 139:173–191, 1984.

A.A. Khalate, X.J.A. Bombois, R. Babuška, H. Wijshoff, and R. Waarsing. Optimization-based feedforward control for a drop-on-demand inkjet printhead. In *American Control Conference, Baltimore, MD, USA*, 2010.

K.S. Kwon. Waveform design methods for piezo inkjet dispensers based on measured meniscus motion. *Journal of Microelectromechanical Systems*, 18 (5):1118–1125, 2009.

K.S. Kwon and W. Kim. A waveform design method for high-speed inkjet printing based on self-sensing measurement. *Sensors and Actuators A: Physical*, 140(1): 75–83, 2007.

C.A. Rabbath. Sensitivity of the discrete- to continuous-time pole transformation at fast sampling rates. Master's thesis, McGill University, Canada, 1995.

M.B.G. Wassink. *Inkjet printhead performance enhancement by feedforward input design based on two-port modeling*. PhD thesis, Delft University of Technology, 2007.

H. Wijshoff. *Structure and fluid-dynamics in piezo inkjet printheads*. PhD thesis, University of Twente, 2008.

C. Williams. Ink-jet printers go beyond paper. *Physics World*, 19:24–29, 2006.

Appendix A. PARAMETRIC UNCERTAINTY

We have to use the information obtained by the identification experiments to describe an uncertainty model for the inkjet system. It is intuitive to present the model uncertainty on the resonant modes of the inkjet system. The properties of the resonant mode i.e. its frequency and damping are well understood in the continuous-time version of a model. Therefore, consider the following continuous-time model of the inkjet channel

$$H(s) = \left(\frac{g_1 s(s+\alpha)}{s^2 + 2\zeta_{n1}\omega_{n1}s + \omega_{n1}^2}\right)\left(\frac{s^2 + 2\zeta_{n3}\omega_{n3}s + \omega_{n3}^2}{s^2 + 2\zeta_{n2}\omega_{n2}s + \omega_{n2}^2}\right). \tag{A.1}$$

It is possible to convert this continues-time model into

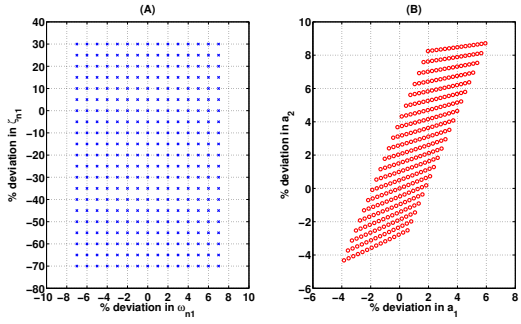

Fig. A.1. Parametric uncertainty in % of nominal value

the discrete-time model given by (2). Based on the identification results we find that the first resonant mode is uncertain. The frequency variation of this mode ω_{n1} is approximately in the interval $[-7\% \ +7\%]$ from its nominal value. The damping ratio variation of this mode ζ_{n1} is approximately in the interval $[-70\% \quad +30\%]$ from its nominal value. These perturbations on ω_{n1} and ζ_{n1} forms a box-type uncertainty as shown in Fig. A.1.A. As a result, the coefficients a_1 and a_2 of $H(q)$ (see (2)) are perturbed from their nominal value when ω_{n1} and ζ_{n1} are perturbed. The parametric uncertainty in the coefficients ω_{n1} and ζ_{n1} of the continuous-time transfer function can be translated into the uncertainty on the coefficients of the discrete-time a_1 and a_2 using standard results [Rabbath, 1995]:

$$a_1 = -2r\cos\theta, \quad a_2 = r^2 \tag{A.2}$$

where $r = e^{-\zeta_{n1}\omega_{n1}T_s}$, $\theta = T_s\omega_{n1}\sqrt{1-\zeta_{n1}^2}$ and T_s is the sampling time. Fig. A.1.B. shows the box-type uncertainty in the parameters ω_{n1} and ζ_{n1} mapped on the parameter space of the coefficient a_1 and a_2. We observe that this is the polytopic uncertainty, which we use for designing the robust actuation pulse. The four vertices of the box-type uncertainty on ω_{n1} and ζ_{n1} are mapped on the parameter space of a_1 and a_2 and these four vertices are $\Delta_1 = [5.93/100 \quad 8.71/100]^T$, $\Delta_2 = [1.96/100 \quad 8.25/100]^T$, $\Delta_3 = [-3.85/100 \quad -4.32/100]^T$, $\Delta_4 = [0.55/100 \quad -2.52/100]^T$. The convex combination of these four vertices form a polytope $\mathbf{\Delta}$ =conv$(\Delta_1, \Delta_2, \Delta_3, \Delta_4)$.

The uncertainty $\Delta = [\Delta^{(1)} \quad \Delta^{(2)}]^T = \sum_{i=1}^4 \alpha_i \Delta_i$ (i.e. $\Delta \in \mathbf{\Delta}$), with $\sum_{i=1}^4 \alpha_i = 1$, will perturb the coefficients a_1 and a_2 in the following manner

$$a_1(\Delta) = a_{1,\text{nom}}(1 + \Delta^{(1)}) \tag{A.3}$$

$$a_2(\Delta) = a_{2,\text{nom}}(1 + \Delta^{(2)}), \tag{A.4}$$

where $a_{1,\text{nom}} = -1.6480$ and $a_{2,\text{nom}} = 0.8839$ are the nominal values of the coefficients a_1 and a_2. It can be observed that the uncertainty $\Delta \in \mathbf{\Delta}$ enters linearly in the perturbed coefficients $a_1(\Delta)$,$a_2(\Delta)$, and thus in the perturbed state-space matrices $A_s(\Delta), B_s(\Delta), C_s(\Delta), D_s(\Delta)$.